JACS
JOURNAL OF THE AMERICAN CHEMICAL SOCIETY
pubs.acs.org/JACS
Article

Interpreting X-ray Diffraction Patterns of Metal−Organic Frameworks via Generative Artificial Intelligence

Bin Feng,[#] Bingxu Wang,[#] Linpeng Lv, Mingzheng Zhang, Zhefeng Chen, Feng Pan,[*] and Shunning Li[*]

Cite This: https://doi.org/10.1021/jacs.5c16416
Read Online

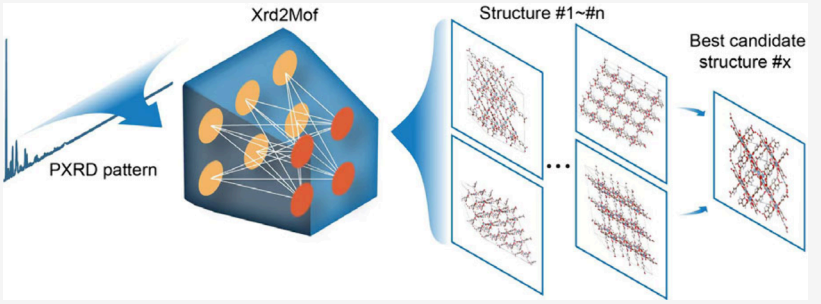

ABSTRACT: Metal−organic frameworks (MOFs) have attracted considerable attention owing to their multifaceted applications and structurally tunable characteristics. Powder X-ray diffraction (XRD) is an essential technique for high-throughput characterization of MOFs. However, it remains challenging to automatically interpret the XRD data due to the diversity and complexity of the geometric structures of MOFs. Herein, we propose a generative artificial intelligence framework based on the Stable-Diffusion architecture for deciphering the structures of MOFs from powder XRD patterns. This model, named as Xrd2Mof, has incorporated domain-specific knowledge by using a coarse-grained representation scheme, which leads to an accuracy of over 93% in identifying the ground truth MOF structure corresponding to the targeted XRD pattern. Xrd2Mof can be directly applied to a diverse range of MOF structures that cover nearly all types of framework topologies, thereby establishing a novel technological avenue for automated structural analysis of MOFs in self-driving laboratories.

INTRODUCTION

Metal−organic frameworks (MOFs) were first introduced by Yaghi et al. in 1995.[1] Since then, research on their design, synthesis, characterization and application has expanded exponentially due to their versatile and tunable nature. MOFs are porous polymeric materials composed of metal nodes and organic linkers connected through coordination interactions to form specific network structures.[2] Their exceptional porosity and high specific surface area have enabled applications in gas storage, separation, and catalysis.[3−11] Recent advances in the synthesis strategies have broadened their applicability to areas such as biomolecular surface coating,[12] optoelectronic memory computing,[13] drug delivery systems,[14] fuel cells and supercapacitors.[15]

The progress in the study of MOFs relies on the design of their structures, which can be accelerated by high-throughput experiments performed by the fully automated robotic laboratories (also known as self-driving laboratories) that have emerged in recent years.[16−18] In this context, X-ray diffraction (XRD) plays a pivotal role in efficiently resolving the crystal structures of MOFs at the atomic scale.[19] Single-crystal XRD (SXRD) was generally employed for definitive structural solutions in previous studies of newly synthesized MOFs, which provides accurate information on atomic positions to enable the complete construction of three-dimensional structures. However, SXRD requires labor-intensive preparation of sufficiently large single crystals and complex refinement procedures, thus limiting its application in high-throughput experimentation.[20−22] In contrast, powder XRD (PXRD) can be used to elucidate the atomic structures of materials under conditions where single crystals are unavailable.[23,24] While PXRD exhibits high compatibility with the automatic MOF synthesis platforms, the information on atomic-level details is typically limited in PXRD patterns of MOFs. The key to applying PXRD in structure identification of MOFs lies in the precise prediction of the framework geometry prior to the indexation of its PXRD pattern, otherwise the overlapping nature of the peaks will prevent us from robust pattern matching.[21,25] At present, we know of no algorithm that can accurately interpret all the structures in

Received: September 18, 2025
Revised: November 26, 2025
Accepted: December 1, 2025

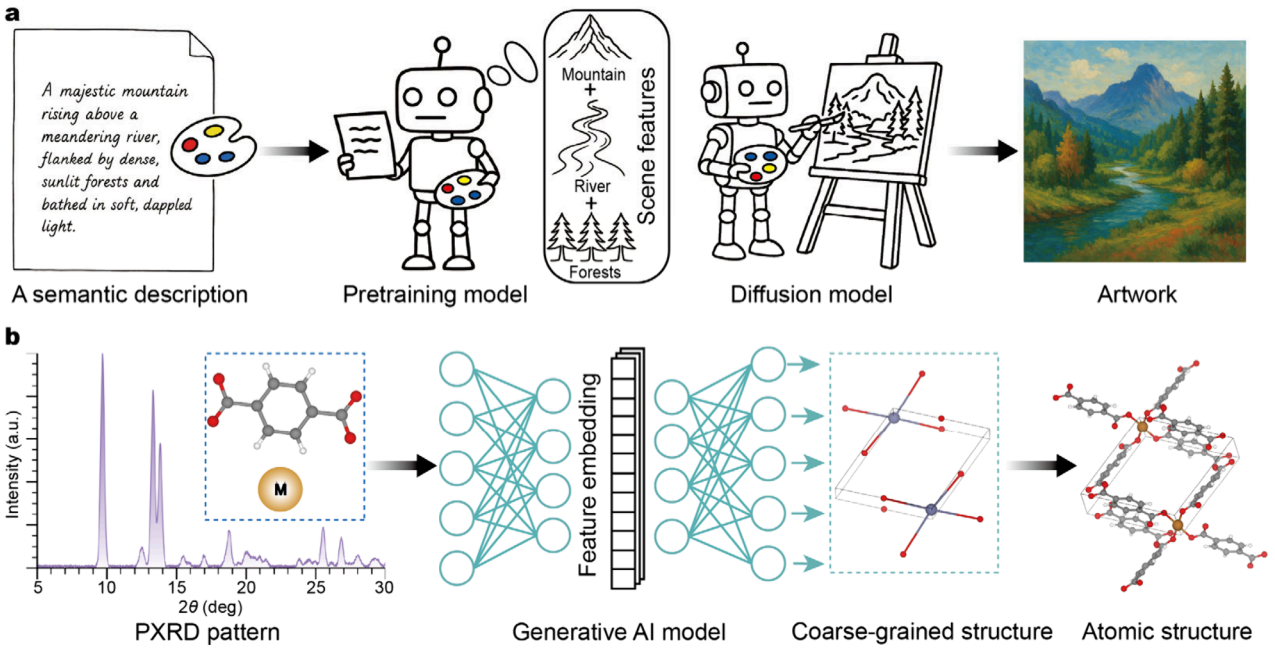

Figure 1. Overview of the generative AI models for the generation of artworks and atomic structures. (a) A typical AI model used to convert textual prompts into artistic painting. During pretraining, a large data set of paired text and images is fed to the model, enabling it to map the patterns of semantic description to visual representation, which optimizes the understanding of scene features. Then, a generative model synthesizes these insights via architectures such as the diffusion model, iteratively refining latent representations to produce an artwork that aligns with the input description. (b) A generative AI model using PXRD pattern to decipher the crystal structure of a MOF synthesized in high-throughput experiments. The compositional information on metal nodes and organic linkers will also serve as input data. The coarse-grained representation, which was proposed to effectively characterize the geometry of MOF skeletons, is employed to facilitate the generation of MOF structures.

MOF family from PXRD data, especially without expert interference such that it can be implemented in the self-driving laboratories.[26,27]

The rapid advancement of artificial intelligence (AI) has demonstrated great potential in resolving the challenge of automated PXRD interpretation.[28] A series of efforts have been previously devoted to phase identification of inorganic compounds from the PXRD data, using algorithms such as convolutional neural networks (CNNs).[29−34] However, due to the complexity of MOF structures, AI models designed for inorganic compounds cannot be directly extended to MOFs. Given that there are several public databases with large-scale structural data of MOFs, such as Cambridge structural database (CSD),[35] CoRE MOF 2019[36] and Reticular Chemistry Structure Resource (RCSR),[37] it has become remarkably convenient to establish AI models for PXRD interpretation of MOFs using synthetic PXRD patterns.[38] Actually, a recent study has developed a model called XtalNet to predict crystal structures based on synthetic PXRD data generated from a simulated MOF data set.[39] However, this model demonstrated efficacy only in a limited set of simulated MOF structures, and there remains a significant gap in prediction accuracy when it is applied to PXRD data of experimental MOF samples.

To tackle the challenge of automated PXRD interpretation of MOFs, we propose a powerful generative AI model that incorporates the domain-specific knowledge into the framework. Naturally, generative models can function as intelligent agents capable of interpreting textual descriptions and generating the corresponding visual images, which typically relies on extensive data sets of paired text-image examples to discern the correlations between descriptive language and visual elements (Figure 1a). In the present work, we treat PXRD pattern as the textual input and MOF structure as the visual output within the framework of a text-to-image model. Leveraging the Stable Diffusion architecture,[40] a generative model named as Xrd2Mof is developed to decipher the MOF structure from PXRD data (Figure 1b). Domain-knowledge-guided coarse-grained representations are utilized to simplify the MOF structures, which carry the key geometric information for PXRD interpretation. By training on a MOF data set of 79,658 entries as extracted from CSD,[41] this model can achieve 93% accuracy in identifying the most probable candidate structure that match with the input PXRD pattern. All known MOF topologies have been covered by the model, which can be readily extended to accommodate larger and more diverse structural classes as needed. Validation tests conducted on experimentally derived PXRD patterns have exhibited excellent performance. Furthermore, we have conducted an analysis of the model interpretability to elucidate how internal feature extraction processes influence the generation of MOF structures. This work provides a foundation for autonomous PXRD-based structural analysis in the design of MOFs.

RESULTS

Architecture of Xrd2Mof. The Xrd2Mof model is composed of three primary phases: feature extraction, coarse-grained structure generation, and building block assembly. During the feature extraction process (Figure 2a), the MOF structures in the training set are represented by the coarse-grained structures via MOFid code,[42] which takes the metal nodes and organic linkers as the building blocks. A multimodal feature extraction approach based on Contrastive Language-Image Pretraining (CLIP)[43] model was developed, with the information on MOF building blocks and XRD pattern serving

https://doi.org/10.1021/jacs.5c16416
J. Am. Chem. Soc. XXXX, XXX, XXX−XXX

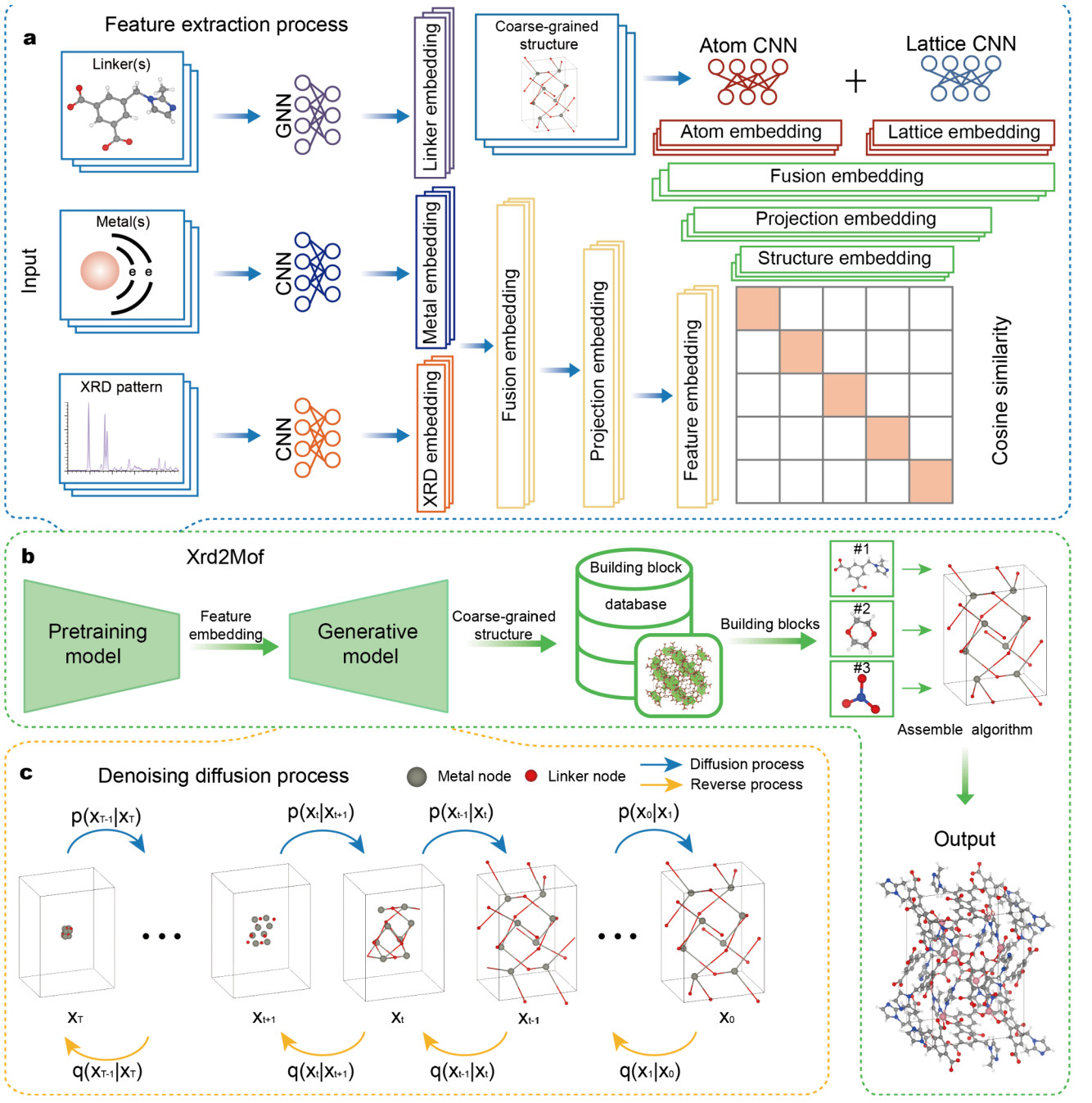

Figure 2. The architecture of the Xrd2Mof. (a) Framework of the pretrained feature extraction model. The model uses input data including simulated XRD patterns, metal nodes, and organic linkers extracted from the structure database. Each feature type is individually processed by dedicated neural networks, whose outputs are combined through a fusion layer and projected into feature vectors via a projection layer. Finally, similarity scores are computed against structural vectors. After training, this module is frozen to provide fixed feature vectors. (b) Overall workflow of Xrd2Mof. Initially, feature extraction is performed to obtain feature vectors, which subsequently guide coarse-grained structural generation. The constructed structures are then matched with building blocks retrieved from the database. Final atomic structures are assembled and optimized using a force-field method. The model captures key structural features and generates candidate structures following predefined chemical principles. Due to inherent stochasticity in the process, multiple candidate structures are produced for further selection. (c) Framework of the structure generation model. The model employs feature vectors as conditions for crystal structure generation. During training, atom valences and types are initialized according to chemical prior knowledge and iteratively refined, guided by feature vectors and diffusion time steps. The generation phase repeats the process in reverse.

as semantic description, and the coarse-grained structures of MOFs as visual representation. For metal nodes, fundamental properties of the metal elements were extracted from the pymatgen[44] library, while for organic linkers, a graph neural network was employed to encode the geometric structures. Information of the simulated XRD pattern was extracted using a CNN model. Different from the previous studies,[39,45−48] we assume that the coordinate information pertaining to organic linkers holds significantly less importance in comparison to that of metal nodes, and consequently, the coordinates of

https://doi.org/10.1021/jacs.5c16416
J. Am. Chem. Soc. XXXX, XXX, XXX−XXX

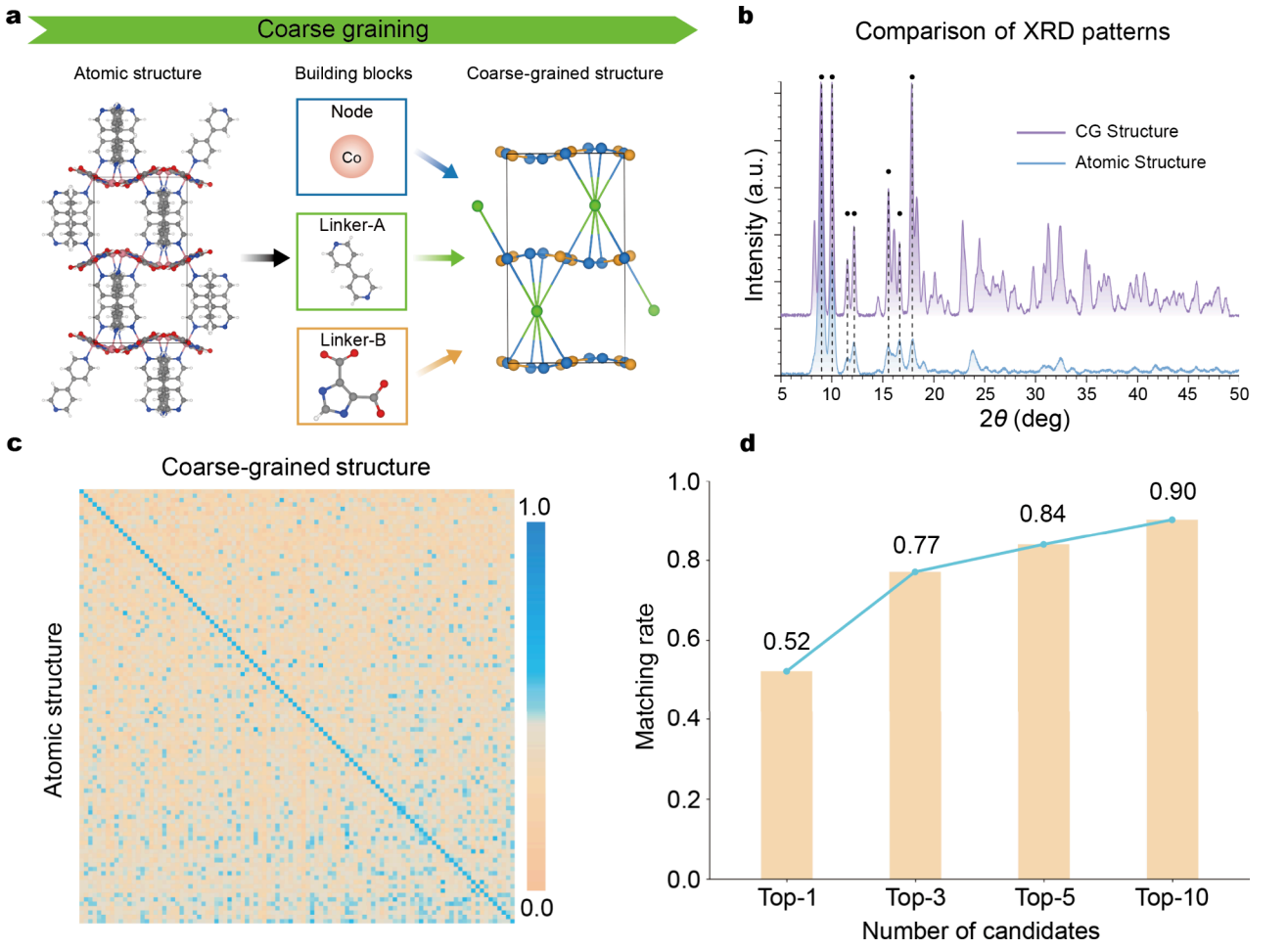

Figure 3. Performance of the pretrained feature extraction model. (a) Illustration of the coarse-graining procedure specifically developed for MOF structures. (b) Comparison between simulated XRD patterns before and after coarse-graining. (c) Confusion matrix obtained from 100 randomly selected structural classes from the test set, where diagonal elements represent correctly classified samples. (d) Matching accuracy of the pretrained model as a function of numbers of candidate structures.

organic linkers were simplified to their centroids. This aligns with our general understanding that the primary peaks in XRD patterns are predominantly attributed to heavy atoms, particularly those belonging to metal nodes. This is the main reason why we use a coarse-grained representation strategy for MOF structures. Here, the atomic positions in coarse-grained representations were abstracted into three-dimensional coordinates of connection points and fed into a CNN (named as Atom CNN), while the unit-cell parameters were fed into another CNN (named as Lattice CNN). The typical cosine similarity was used as the matching scheme in CLIP to compare the embeddings of such semantic description and visual representation.

After feature extraction, a generative model was employed to generate the coarse-grained structure for a targeted XRD pattern along with the corresponding information on building blocks as additional inputs (Figure 2b). We adopted the Stable Diffusion architecture from MOFdiff,[49] which can directly incorporate the above embeddings into the structure generation process (Figure 2c). To determine the number of connection points, the charge conservation principle was applied to establish minimal metal-to-linker ratios, in which the valence states of metal ions were explicitly specified according to experimental precursors, while the valence states of organic linkers were deduced based on a mapping table from SMILES strings to standard valence-specific linker units in a comprehensive database. We note that during the training of this generative model, the positions of metal nodes were prioritized over the organic linkers in input vectors, which can facilitate the assembly of building blocks in a more rational manner as guided by the XRD patterns.

Finally, in the building block assembly process, we have established a database containing approximately 400,000 building blocks and organized them into a K-Dimensional Tree search library indexed by the Extended Connectivity FingerPrints (ECFP). For single-linker MOFs (~60% of our data set), the organic linkers were proportionally and sequentially allocated to the connection points in coarse-grained structures. For dual-linker MOFs (~26% of the data set), linker distribution was explicitly predicted via Ewald summation method, which can identify the most energetically favorable configurations among the extensive combinatorial possibilities. Afterward, we used ten candidate structures for further optimization via Universal Force Field (UFF), generating physically plausible MOF structures as the output of Xrd2Mof.

Model Performance. The CLIP model serves as the foundation for subsequent structure generation and assembly processes, and thus it is of paramount importance in ensuring its reliability. We note that only coarse-grained structures

https://doi.org/10.1021/jacs.5c16416
J. Am. Chem. Soc. XXXX, XXX, XXX−XXX

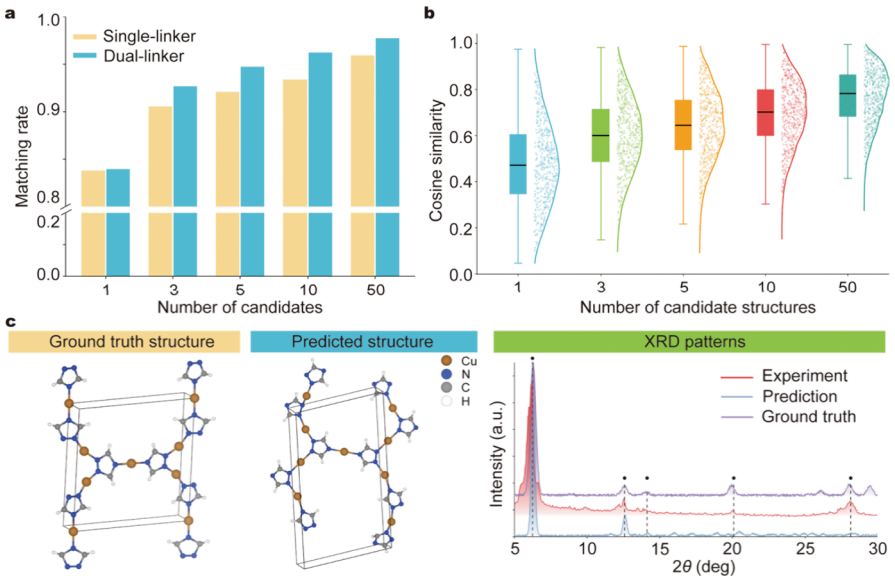

Figure 4. Performance of the structure generation model. (a) Main-peak matching rates for single-linker and dual-linker MOFs upon matching different numbers of candidate structures. (b) Distribution of cosine similarity between the predicted and real XRD patterns upon matching different numbers of candidate structures. (c) Structure generation from real experimental data, and the corresponding XRD patterns (ground truth XRD pattern corresponds to the one directly simulated from the ground truth MOF structure).

containing fewer than 50 connection points were taken into consideration in our model, corresponding to 99% of all the MOF structures in the database. MOF structures containing hundreds and even thousands of atoms can be included in the model (Figure 3a), which significantly surpasses that of the previous report.[39] Simulated XRD patterns of coarse-grained structures exhibited high fidelity to those of atomic structures, confirming the reliable extraction of essential diffraction features (Figure 3b). Differences in peak splitting are observed, which is likely due to the negligence of atomic detail in organic linkers. To ensure robust model generalization, the training data set was augmented by random functionalization of linker structures and substitution of metal nodes (Table S1, S2, and Figure S1). By evaluating the feature extraction performance on a test set containing ~ 10,000 MOFs, we generated encoded features and identified the top 10 most similar MOFs for each query structure, achieving an average matching accuracy of 90.3%, demonstrating outstanding classification performance (Figures 3c,d).

The stochastic nature of Stable Diffusion model implies that an increased number of candidate structures could correspondingly increase the likelihood of reproducing the ground truth crystal structure. Therefore, four primitive structures were generated with various numbers of connection points satisfying charge-neutrality rules, subsequently producing a series of candidate crystal structures. To quantify the prediction accuracy, we implement a main-peak matching scheme, in which the primary diffraction peaks in the targeted XRD pattern are compared to those calculated from the candidate structures, using a predefined angular tolerance to ensure that each peak is matched only once. We establish a threshold wherein the two XRD patterns can be considered identical when a minimum of ten peaks exhibit a high degree of alignment (Figure S2). Figure 4a shows the success rates of Xrd2Mof for single-linker and dual-linker MOFs upon matching different numbers of candidate structures. Here, the success rate is defined as the proportion of test-set samples for which at least one predicted candidate MOF structure yields an XRD pattern that matches well with the simulated XRD pattern of the ground-truth structure. We note that upon matching 10 candidate structures, success rates of 93.4% and 96.2% are achieved for single-linker and dual-linker species, respectively, which are close to that of matching 50 candidate structures. Surprisingly, dual-linker systems demonstrate slightly higher success rates as compared to their single-linker counterparts. This can be attributed to the fact that the fitting accuracy of deep generative models tends to increase with the number of independent variables, which corresponds to a more expressive representation space (Figure S3). We note that high matching rates are also obtained based on the average cosine similarity values between the targeted XRD pattern and the simulated ones of the candidate structures (Figure 4b). Consequently, we use the results of 10 candidate structures as the final output of Xrd2Mof. It is also noteworthy that the primary diffraction peaks mainly locate in the low-angle region (2θ ranging from 5° to 30°, shown in Figure S4 and S5), rendering the main-peak matching scheme more reliable than the cosine similarity scheme in comparing two XRD patterns. Therefore, we employ the former one to evaluate the model performance in this study.

To further optimize model performance, multiple architectural configurations and XRD processing strategies have been evaluated, along with the assessments of different candidate numbers used in Ewald summation calculations (Figure S6). Since the model is trained on simulated XRD patterns, it is probable that its performance will be reduced when applied on experimental results. However, as exemplified by one of the reported XRD pattern (CSD ID: ALICEE)[50] shown in Figure 4c, the generated MOF structure exhibits high similarity to the ground truth structure, despite minor angular discrepancies between the predicted and the real XRD patterns. We note that some additional peaks emerge in the predicted XRD pattern, which is likely attributable to the error of linker orientation as predicted in the building block assembly process. Nevertheless, it is evident that Xrd2Mof can provide highly

https://doi.org/10.1021/jacs.5c16416
J. Am. Chem. Soc. XXXX, XXX, XXX−XXX

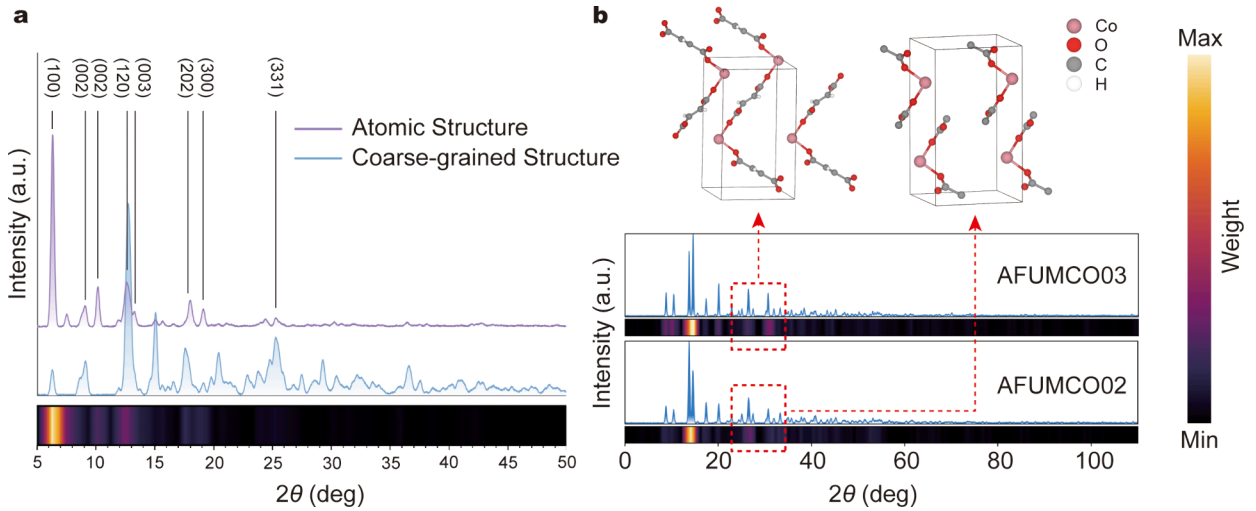

Figure 5. Grad-CAM analysis of the feature extraction process. (a) XRD patterns and Grad-CAM heatmap for ABADUG in the test set. (b) XRD patterns and the corresponding Grad-CAM heatmaps for two MOFs with the same building blocks but different distributions.

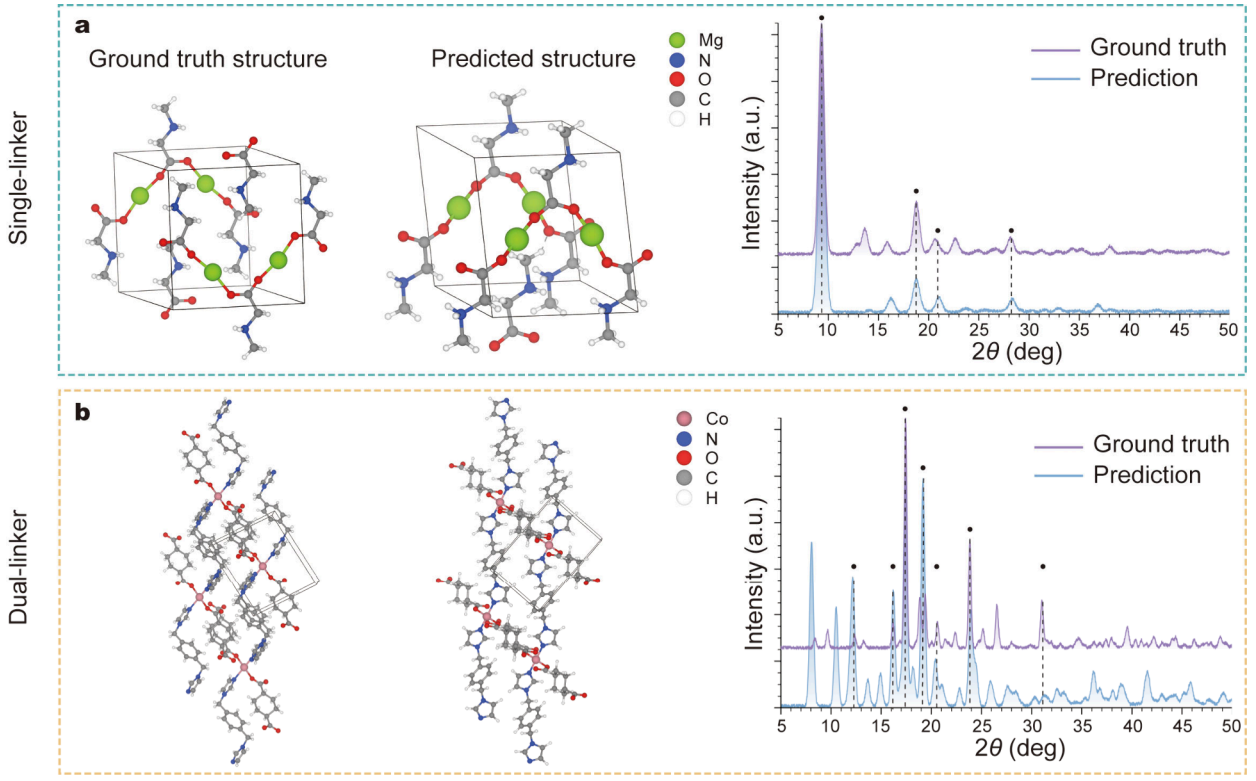

Figure 6. Comparison of framework topology in the structure generation process. (a) Structure generation result of a single-linker MOF, and the corresponding simulated XRD patterns. The highlighted peaks in XRD patterns are associated with the framework structure. (b) Structure generation result of a dual-linker MOF, and the corresponding simulated XRD patterns.

accurate and robust structure generation results from the experimental XRD patterns of MOFs.

Role of Coarse Graining. Here, we examine the significance of coarse-grained representation of MOFs in the predictive power of Xrd2Mof. Gradient-weighted Class Activation Mapping (Grad-CAM)[51] is employed to facilitate this analysis, which can help assess whether the prediction accuracy arises from capturing the discriminative features or from overfitting to artifacts in the data.[52,53] Grad-CAM can visualize the attention distribution of a trained convolutional architecture. When applied to XRD patterns, it highlights the most discriminative 2θ regions, thereby elucidating the decision-making process of the CLIP model in Xrd2Mof.

We have randomly selected a MOF structure from CSD (ID: ABADUG[54]), as displayed in Figure 5a. Notably, the primary diffraction peaks simulated from its coarse-grained structure closely correspond to those simulated from its atomic structure, indicating that coarse graining can effectively retain most of the structure-relevant characteristics inherent in the XRD patterns. The Grad-CAM map shows substantially high attention on these primary diffraction peaks, demonstrating that the feature extraction process (i.e., the CLIP model) can

https://doi.org/10.1021/jacs.5c16416
J. Am. Chem. Soc. XXXX, XXX, XXX−XXX

successfully capture the most crucial 2θ regions for XRD interpretation. This result suggests the critical role of coarse graining in mapping the relationship connecting an XRD pattern and the corresponding MOF structure. We have also compared two MOFs with the same building blocks, as shown in Figure 5b. The distribution of organic linkers exhibits distinct patterns between these two structures, whereas the distribution of metal nodes is relatively similar. This leads to only minor discrepancies in XRD patterns, mainly characterized by variations in the secondary peaks. Nevertheless, the Grad-CAM maps indicate that the CLIP model can successfully discern these discrepancies, which is likely due to the difference in coarse-grained structures for both MOFs. The above results indicate that the high accuracy of the CLIP model is closely associated with the coarse-grained representation scheme.

The significance of coarse graining in the structure generation process of Xrd2Mof can be illustrated by the two examples shown in Figure 6. The coarse-grained structure contains the information about framework topology while discarding the information on atomic positions within the building blocks. This leads to a substantially reduced degrees of freedom, potentially facilitating the model's ability to discern the inherent mapping between XRD patterns and MOF structures. We note that the training data set in our work remains inadequate to directly generate the atomic positions of a crystal structure comprising hundreds of atoms, which is the prevalent scenario for most MOFs in CSD. By using coarse graining, the model focuses on the positions of building blocks rather than atoms, and consequently the data on MOF structures are compressed by about an order of magnitude. This strategy can enable the diffusion model to accurately reproduce the local connectivity of building blocks (i.e., framework topology) in the ground truth structure. For the single-linker example shown in Figure 6a, the predicted structure matches well with the ground truth structure in that each metal node is connected to two organic linkers, and each linker binds with two metal ions. This consistency in framework topology results in a striking similarity between the predicted and ground truth XRD patterns. For the dual-linker case in Figure 6b, the Ewald summation method employed in the assembly process facilitates the coarse-grained representation scheme, thereby enabling the generation of a MOF structure that retains the same framework topology as the ground truth. Despite the apparent discrepancy in the conformation of organic linkers, the predicted XRD pattern exhibits a high degree of consistency with the ground truth pattern. These results demonstrate that the coarse-grained representation scheme is essential in a generative model to interpret the XRD patterns of MOFs.

DISCUSSION

Automated self-driving laboratories are transforming the traditional trial-and-error paradigm by enabling continuous data-driven and feedback-controlled experimentation. Through the integration of robotics, machine learning and real-time data analytics, these systems can autonomously design, synthesize and characterize materials with minimal human intervention, substantially improving both the efficiency and reproducibility of research workflows. Nowadays, significant achievements have been made in the field of inorganic materials and organic molecules.[55−57] Analogous to the models designed for inorganic compounds, generative AI models for MOFs typically employ existing structure databases to simulate the target property or characterization. They generally encounter a substantial limitation on the maximum number of atoms in the MOF structure, rendering them incapable of encompassing numerous experimentally observed samples. Xrd2Mof addresses this challenge by explicitly incorporating a coarse graining strategy, which provides chemical prior knowledge to facilitate the feature extraction and structure generation processes, finally resulting in promising accuracy in interpreting the XRD patterns for nearly all MOFs in CSD. This advantage positions Xrd2Mof as a useful component in automated self-driving laboratories for the development of MOFs. By reconstructing the atomic structures directly from readily accessible PXRD data in high-throughput synthesis experiments, Xrd2Mof can substantially expedite the experimentation process, thereby enhancing efficiency in the discovery of MOFs with exceptional performance. More importantly, since Xrd2Mof covers nearly all kinds of framework topologies, it can be seamlessly integrated into the existing high-throughput pipelines for various MOFs.

It is noteworthy that the practical implementation of this model assumes the availability of structural information for the precursor metal and linker components employed during MOF synthesis, particularly the elemental identities of the metal nodes and the SMILES strings of the organic linkers. While the compositional information on metal nodes is readily available prior to synthesis, it is crucial to emphasize that the information on organic molecules in precursors can also be employed as reliable inputs for the linkers in MOFs. This is due to the fact that organic linkers usually do not decompose during the synthesis of MOFs, which generally requires mild conditions well below the thermal decomposition temperatures of most linkers. Organic molecules in the precursors can retain their molecular integrity and form the framework by coordinating with metal ions or clusters via coordination bonds. Specifying the constituents of metal nodes and the structures of organic linkers can direct the generative model toward more plausible chemical space, thereby limiting the effective search space from all conceivable structures to a more feasible subset. Such strategy can significantly reduce the probability of generating chemically unreasonable configurations and thus improve the prediction accuracy of the model. Moreover, as mentioned above, the sharp peaks in PXRD patterns of MOFs generally correspond to the metal-to-metal distances and unit cell dimensions, while organic linkers contribute little intensity. The structural information on organic linkers serving as inputs to the model can successfully complement this inherent deficiency in PXRD interpretation.

Nevertheless, there are still some limitations in Xrd2Mof. First, in the absence of reliable information on the metal and linker components, the model is incapable of generating a structure corresponding to the target PXRD pattern. There are still instances where organic linkers undergo in situ reactions or decomposition to form new species during MOF synthesis. Although these reactions are typically intentionally designed rather than occurring accidentally, it is crucial to provide the correct SMILES strings, as otherwise the predictions of MOF structures will be inaccurate. Second, many MOFs are synthesized in specific solution environments, and their experimental XRD patterns typically contain unavoidable impurity signals. Xrd2Mof does not account for these solvent molecules, even though they can be present in MOF structures. This is because incorporating these molecules

https://doi.org/10.1021/jacs.5c16416
J. Am. Chem. Soc. XXXX, XXX, XXX−XXX

(most of them do not belong to the framework topology) into the model during training would significantly reduce model accuracy in structure generation. Nevertheless, we have explicitly examined the model's robustness by conducting tests on the simulated PXRD patterns where impurity peaks are superimposed over those of the pristine sample. The results shown in Figure S7 and S8 demonstrate that the overall matching success rate can still reach 90.6% for the generation of MOF structures. Third, the validation of experimental XRD patterns remains insufficient. Active learning loops are therefore warranted for future studies to incorporate more experimental data into the training of Xrd2Mof.

CONCLUSION

This work introduces Xrd2Mof, a generative AI model designed to reconstruct the crystal structures directly from PXRD patterns of MOFs. Xrd2Mof can be seamlessly integrated into high-throughput experimental pipelines, effectively bridging the gap between material characterization and structural interpretation. By employing the coarse graining strategy, the model can be directly applied to a diverse range of MOF structures without the requirement for retraining, achieving a balance between accuracy and computational efficiency. Upon matching 10 candidate structures, an overall success rate of >93% is achieved for interpreting the XRD patterns of both single-linker and dual-linker MOFs. The findings presented in this research can be readily extended beyond XRD patterns, potentially to characterization techniques such as infrared, Raman, or nuclear magnetic resonance spectra, thus providing a foundation for future studies on the integration of multimodal techniques in self-driving laboratories.

ASSOCIATED CONTENT

Data Availability Statement

The data is available from https://zenodo.org/records/15745443. Code is available from https://github.com/PKUsam2023/Xrd2Mof.

Supporting Information

The Supporting Information is available free of charge at https://pubs.acs.org/doi/10.1021/jacs.5c16416.

Detailed methods used in Xrd2Mof, data augmentation techniques, XRD pattern matching threshold, explanation of the success rate, inputs for feature extraction, performance optimization strategies, tests conducted on impurity signals (PDF)

AUTHOR INFORMATION

Corresponding Authors

Feng Pan − *School of Advanced Materials, Peking University, Shenzhen Graduate School, Shenzhen 518055, P. R. China;* orcid.org/0000-0002-8216-1339; Email: panfeng@pkusz.edu.cn

Shunning Li − *School of Advanced Materials, Peking University, Shenzhen Graduate School, Shenzhen 518055, P. R. China;* orcid.org/0000-0002-5381-6025; Email: lisn@pku.edu.cn

Authors

Bin Feng − *School of Advanced Materials, Peking University, Shenzhen Graduate School, Shenzhen 518055, P. R. China;* orcid.org/0009-0003-1642-9776

Bingxu Wang − *School of Advanced Materials, Peking University, Shenzhen Graduate School, Shenzhen 518055, P. R. China*

Linpeng Lv − *School of Advanced Materials, Peking University, Shenzhen Graduate School, Shenzhen 518055, P. R. China*

Mingzheng Zhang − *School of Advanced Materials, Peking University, Shenzhen Graduate School, Shenzhen 518055, P. R. China*

Zhefeng Chen − *School of Advanced Materials, Peking University, Shenzhen Graduate School, Shenzhen 518055, P. R. China*

Complete contact information is available at: https://pubs.acs.org/10.1021/jacs.5c16416

Author Contributions

#These authors contributed equally: Bin Feng, Bingxu Wang.

Notes

The authors declare no competing financial interest.

ACKNOWLEDGMENTS

The authors acknowledge financial support from the Basic and Applied Basic Research Foundation of Guangdong Province (2023A1515011391 and 2021B1515130002), Guangdong Key Laboratory of Design and Calculation of New Energy Materials (No. 2017B030301013), Shenzhen Key Laboratory of New Energy Resources Genome Preparation and Testing (No. ZDSYS201707281026184), National Center for International Research of Power Batteries and Materials (No. 2015B01015) and the Major Science and Technology Infrastructure Project of Material Genome Big-science Facilities Platform supported by Municipal Development and Reform Commission of Shenzhen.

REFERENCES

(1) Yaghi, O. M.; Li, H. Hydrothermal synthesis of a metal-organic framework containing large rectangular channels. *J. Am. Chem. Soc.* **1995**, *117* (41), 10401−10402.

(2) James, S. L. Metal-organic frameworks. *Chem. Soc. Rev.* **2003**, *32* (5), 276−288.

(3) Dan, W.; Wei, G.; Fang, X. Three-Dimensional Hydrogen-Bonded Porous Metal-Organic Framework for Natural Gas Separation with High Selectivity. *Molecules* **2024**, *29* (2), 424.

(4) Elsaidi, S. K.; Mohamed, M. H.; Helal, A. S.; Galanek, M.; Pham, T.; Suepaul, S.; Space, B.; Hopkinson, D.; Thallapally, P. K.; Li, J. Radiation-resistant metal-organic framework enables efficient separation of krypton fission gas from spent nuclear fuel. *Nat. Commun.* **2020**, *11* (1), 3103.

(5) Furukawa, H.; Cordova, K. E.; O'Keeffe, M.; Yaghi, O. M. The chemistry and applications of metal-organic frameworks. *Science* **2013**, *341* (6149), 1230444.

(6) Huang, D.-S.; Qiu, X.-F.; Huang, J.-R.; Mao, M.; Liu, L.; Han, Y.; Zhao, Z.-H.; Liao, P.-Q.; Chen, X.-M. Electrosynthesis of urea by using Fe2O3 nanoparticles encapsulated in a conductive metal-organic framework. *Nature Synthesis* **2024**, *3* (11), 1404−1413.

(7) Liu, J.; Chen, L.; Cui, H.; Zhang, J.; Zhang, L.; Su, C.-Y. Applications of metal-organic frameworks in heterogeneous supramolecular catalysis. *Chem. Soc. Rev.* **2014**, *43* (16), 6011−6061.

(8) Mo, R.-J.; Chen, S.; Huang, L.-Q.; Ding, X.-L.; Rafique, S.; Xia, X.-H.; Li, Z.-Q. Regulating ion affinity and dehydration of metal-organic framework sub-nanochannels for high-precision ion separation. *Nat. Commun.* **2024**, *15* (1), 2145.

(9) Xu, Y.; Li, Q.; Xue, H.; Pang, H. Metal-organic frameworks for direct electrochemical applications. *Coord. Chem. Rev.* **2018**, *376*, 292−318.

(10) Yaghi, O. M.; O'Keeffe, M.; Ockwig, N. W.; Chae, H. K.; Eddaoudi, M.; Kim, J. Reticular synthesis and the design of new materials. *Nature* **2003**, *423* (6941), 705−714.
(11) Yang, C.; Shang, S.; Lin, L.; Wang, P.; Ye, Z.; Wang, Y.; Shih, K.; Sun, L.; Li, X.-y. Electro-driven cycling Fenton catalysis through two-dimensional electroresponsive metal-organic frameworks for water purification. *Nature Water* **2024**, *2* (8), 793−802.
(12) Liang, K.; Ricco, R.; Doherty, C. M.; Styles, M. J.; Bell, S.; Kirby, N.; Mudie, S.; Haylock, D.; Hill, A. J.; Doonan, C. J.; et al. Biomimetic mineralization of metal-organic frameworks as protective coatings for biomacromolecules. *Nat. Commun.* **2015**, *6* (1), 7240.
(13) Bachinin, S. V.; Marunchenko, A.; Matchenya, I.; Zhestkij, N.; Shirobokov, V.; Gunina, E.; Novikov, A.; Timofeeva, M.; Povarov, S. A.; Li, F.; et al. Metal-organic framework single crystal for in-memory neuromorphic computing with a light control. *Communications Materials* **2024**, *5* (1), 128.
(14) Cai, W.; Wang, J.; Chu, C.; Chen, W.; Wu, C.; Liu, G. Metal-organic framework-based stimuli-responsive systems for drug delivery. *Advanced Science* **2019**, *6* (1), 1801526.
(15) Mehtab, T.; Yasin, G.; Arif, M.; Shakeel, M.; Korai, R. M.; Nadeem, M.; Muhammad, N.; Lu, X. Metal-organic frameworks for energy storage devices: Batteries and supercapacitors. *Journal of Energy Storage* **2019**, *21*, 632−646.
(16) Tom, G.; Schmid, S. P.; Baird, S. G.; Cao, Y.; Darvish, K.; Hao, H.; Lo, S.; Pablo-García, S.; Rajaonson, E. M.; Skreta, M.; et al. Self-driving laboratories for chemistry and materials science. *Chem. Rev.* **2024**, *124* (16), 9633−9732.
(17) Arslan, H. K.; Shekhah, O.; Wohlgemuth, J.; Franzreb, M.; Fischer, R. A.; Wöll, C. High-throughput fabrication of uniform and homogenous MOF coatings. *Adv. Funct. Mater.* **2011**, *21* (22), 4228−4231.
(18) Biemmi, E.; Christian, S.; Stock, N.; Bein, T. High-throughput screening of synthesis parameters in the formation of the metal-organic frameworks MOF-5 and HKUST-1. *Microporous Mesoporous Mater.* **2009**, *117* (1−2), 111−117.
(19) Payam, A. F.; Khalil, S.; Chakrabarti, S. Synthesis and characterization of MOF-derived structures: Recent advances and future perspectives. *Small* **2024**, *20* (32), 2310348.
(20) Kaduk, J. A.; Billinge, S. J. L.; Dinnebier, R. E.; Henderson, N.; Madsen, I.; Černý, R.; Leoni, M.; Lutterotti, L.; Thakral, S.; Chateigner, D. Powder diffraction. *Nature Reviews Methods Primers* **2021**, *1* (1), 77.
(21) Martí-Rujas, J. Structural elucidation of microcrystalline MOFs from powder X-ray diffraction. *Dalton Transactions* **2020**, *49* (40), 13897−13916.
(22) Subudhi, S.; Tripathy, S. P.; Parida, K. Highlights of the characterization techniques on inorganic, organic (COF) and hybrid (MOF) photocatalytic semiconductors. *Catalysis Science & Technology* **2021**, *11* (2), 392−415.
(23) Férey, G.; Mellot-Draznieks, C.; Serre, C.; Millange, F.; Dutour, J.; Surblé, S.; Margiolaki, I. A chromium terephthalate-based solid with unusually large pore volumes and surface area. *Science* **2005**, *309* (5743), 2040−2042.
(24) Stern, L. A.; Kirby, S. H.; Durham, W. B. Peculiarities of methane clathrate hydrate formation and solid-state deformation, including possible superheating of water ice. *Science* **1996**, *273* (5283), 1843−1848.
(25) Li, S.; Wu, X.; Pan, Q.; Cheng, Q.; Li, H. Comparison of the accuracy of powder and single-crystal X-ray diffraction techniques in determining organic crystal structure. *Chin. Sci. Bull.* **2014**, *59*, 497−501.
(26) Hirschle, P.; Preiß, T.; Auras, F.; Pick, A.; Völkner, J.; Valdepérez, D.; Witte, G.; Parak, W. J.; Rädler, J. O.; Wuttke, S. Exploration of MOF nanoparticle sizes using various physical characterization methods-is what you measure what you get? *CrystEngComm* **2016**, *18* (23), 4359−4368.
(27) Howarth, A. J.; Peters, A. W.; Vermeulen, N. A.; Wang, T. C.; Hupp, J. T.; Farha, O. K. Best practices for the synthesis, activation, and characterization of metal-organic frameworks. *Chem. Mater.* **2017**, *29* (1), 26−39.
(28) Wang, H.; Fu, T.; Du, Y.; Gao, W.; Huang, K.; Liu, Z.; Chandak, P.; Liu, S.; Van Katwyk, P.; Deac, A.; et al. Scientific discovery in the age of artificial intelligence. *Nature* **2023**, *620* (7972), 47−60.
(29) Oviedo, F.; Ren, Z.; Sun, S.; Settens, C.; Liu, Z.; Hartono, N. T. P.; Ramasamy, S.; DeCost, B. L.; Tian, S. I.; Romano, G.; et al. Fast and interpretable classification of small X-ray diffraction datasets using data augmentation and deep neural networks. *npj Computational Materials* **2019**, *5* (1), 60.
(30) Massuyeau, F.; Broux, T.; Coulet, F.; Demessence, A.; Mesbah, A.; Gautier, R. Perovskite or Not Perovskite? A Deep-Learning Approach to Automatically Identify New Hybrid Perovskites from X-ray Diffraction Patterns. *Adv. Mater.* **2022**, *34* (41), 2203879.
(31) Wang, H.; Xie, Y.; Li, D.; Deng, H.; Zhao, Y.; Xin, M.; Lin, J. Rapid identification of X-ray diffraction patterns based on very limited data by interpretable convolutional neural networks. *J. Chem. Inf. Model.* **2020**, *60* (4), 2004−2011.
(32) Chen, Z.; Xie, Y.; Wu, Y.; Lin, Y.; Tomiya, S.; Lin, J. An interpretable and transferrable vision transformer model for rapid materials spectra classification. *Digital Discovery* **2024**, *3* (2), 369−380.
(33) Chen, D.; Bai, Y.; Ament, S.; Zhao, W.; Guevarra, D.; Zhou, L.; Selman, B.; van Dover, R. B.; Gregoire, J. M.; Gomes, C. P. Automating crystal-structure phase mapping by combining deep learning with constraint reasoning. *Nature Machine Intelligence* **2021**, *3* (9), 812−822.
(34) Riesel, E. A.; Mackey, T.; Nilforoshan, H.; Xu, M.; Badding, C. K.; Altman, A. B.; Leskovec, J.; Freedman, D. E. Crystal structure determination from powder diffraction patterns with generative machine learning. *J. Am. Chem. Soc.* **2024**, *146* (44), 30340−30348.
(35) Moghadam, P. Z.; Li, A.; Liu, X.-W.; Bueno-Perez, R.; Wang, S.-D.; Wiggin, S. B.; Wood, P. A.; Fairen-Jimenez, D. Targeted classification of metal-organic frameworks in the Cambridge structural database (CSD). *Chemical science* **2020**, *11* (32), 8373−8387.
(36) Chung, Y. G.; Haldoupis, E.; Bucior, B. J.; Haranczyk, M.; Lee, S.; Zhang, H.; Vogiatzis, K. D.; Milisavljevic, M.; Ling, S.; Camp, J. S.; et al. Advances, updates, and analytics for the computation-ready, experimental metal-organic framework database: CoRE MOF 2019. *Journal of Chemical & Engineering Data* **2019**, *64* (12), 5985−5998.
(37) O'keeffe, M.; Peskov, M. A.; Ramsden, S. J.; Yaghi, O. M. The reticular chemistry structure resource (RCSR) database of, and symbols for, crystal nets. *Accounts of chemical research* **2008**, *41* (12), 1782−1789.
(38) Wilmer, C. E.; Leaf, M.; Lee, C. Y.; Farha, O. K.; Hauser, B. G.; Hupp, J. T.; Snurr, R. Q. Large-scale screening of hypothetical metal-organic frameworks. *Nature Chem.* **2012**, *4* (2), 83−89.
(39) Lai, Q.; Xu, F.; Yao, L.; Gao, Z.; Liu, S.; Wang, H.; Lu, S.; He, D.; Wang, L.; Zhang, L.; et al. End-to-End Crystal Structure Prediction from Powder X-Ray Diffraction. *Advanced Science* **2025**, *12* (8), 2410722.
(40) Rombach, R.; Blattmann, A.; Lorenz, D.; Esser, P.; Ommer, B. High-resolution image synthesis with latent diffusion models. In *Proceedings of the IEEE/CVF conference on computer vision and pattern recognition*, 2022; pp 10684−10695.
(41) Groom, C. R.; Bruno, I. J.; Lightfoot, M. P.; Ward, S. C. The Cambridge structural database. *Structural Science* **2016**, *72* (2), 171−179.
(42) Bucior, B. J.; Rosen, A. S.; Haranczyk, M.; Yao, Z.; Ziebel, M. E.; Farha, O. K.; Hupp, J. T.; Siepmann, J. I.; Aspuru-Guzik, A.; Snurr, R. Q. Identification schemes for metal-organic frameworks to enable rapid search and cheminformatics analysis. *Cryst. Growth Des.* **2019**, *19* (11), 6682−6697.
(43) Radford, A.; Kim, J. W.; Hallacy, C.; Ramesh, A.; Goh, G.; Agarwal, S.; Sastry, G.; Askell, A.; Mishkin, P.; Clark, J. Learning transferable visual models from natural language supervision. In *International conference on machine learning*, 2021; PmLR *139*, pp 8748−8763.

https://doi.org/10.1021/jacs.5c16416
J. Am. Chem. Soc. XXXX, XXX, XXX−XXX

(44) Ong, S. P.; Richards, W. D.; Jain, A.; Hautier, G.; Kocher, M.; Cholia, S.; Gunter, D.; Chevrier, V. L.; Persson, K. A.; Ceder, G. Python Materials Genomics (pymatgen): A robust, open-source python library for materials analysis. *Comput. Mater. Sci.* **2013**, *68*, 314−319.
(45) Hoogeboom, E.; Satorras, V. G.; Vignac, C.; Welling, M. Equivariant diffusion for molecule generation in 3d. In *International conference on machine learning*, 2022; PMLR *162*, pp 8867−8887.
(46) Jiao, R.; Huang, W.; Lin, P.; Han, J.; Chen, P.; Lu, Y.; Liu, Y. Crystal structure prediction by joint equivariant diffusion. *Advances in Neural Information Processing Systems* **2023**, *36*, 17464−17497.
(47) Park, H.; Yan, X.; Zhu, R.; Huerta, E. A.; Chaudhuri, S.; Cooper, D.; Foster, I.; Tajkhorshid, E. A generative artificial intelligence framework based on a molecular diffusion model for the design of metal-organic frameworks for carbon capture. *Communications Chemistry* **2024**, *7* (1), 21.
(48) Zeni, C.; Pinsler, R.; Zügner, D.; Fowler, A.; Horton, M.; Fu, X.; Wang, Z.; Shysheya, A.; Crabbé, J.; Ueda, S.; et al. A generative model for inorganic materials design. *Nature* **2025**, *639*, 624−632.
(49) Fu, X.; Xie, T.; Rosen, A. S.; Jaakkola, T.; Smith, J. Mofdiff: Coarse-grained diffusion for metal-organic framework design. *arXiv preprint arXiv:2310.10732* 2023.
(50) Huang, Y. G.; Mu, B.; Schoenecker, P. M.; Carson, C. G.; Karra, J. R.; Cai, Y.; Walton, K. S. A porous flexible homochiral SrSi2 array of single-stranded helical nanotubes exhibiting single-crystal-to-single-crystal oxidation transformation. *Angew. Chem. Int. Ed.* **2011**, *50* (2), 436−440.
(51) Selvaraju, R. R.; Cogswell, M.; Das, A.; Vedantam, R.; Parikh, D.; Batra, D. Grad-cam: Visual explanations from deep networks via gradient-based localization. In *Proceedings of the IEEE international conference on computer vision*, 2017; pp 618−626.
(52) Montavon, G.; Samek, W.; Müller, K.-R. Methods for interpreting and understanding deep neural networks. *Digital signal processing* **2018**, *73*, 1−15.
(53) Zhang, Y.; Tiňo, P.; Leonardis, A.; Tang, K. A survey on neural network interpretability. *IEEE transactions on emerging topics in computational intelligence* **2021**, *5* (5), 726−742.
(54) Wang, J.; Cheng, Y.; Zhou, J.; Tang, W. A donor-acceptor liganded metal-organic framework showcases the hydrogen-bond-enhanced sensing of N-heterocyclic explosives. *Journal of Materials Chemistry C* **2021**, *9* (36), 12086−12093.
(55) Dai, T.; Vijayakrishnan, S.; Szczypiński, F. T.; Ayme, J.-F.; Simaei, E.; Fellowes, T.; Clowes, R.; Kotopanov, L.; Shields, C. E.; Zhou, Z.; et al. Autonomous mobile robots for exploratory synthetic chemistry. *Nature* **2024**, *635* (8040), 890−897.
(56) Szymanski, N. J.; Rendy, B.; Fei, Y.; Kumar, R. E.; He, T.; Milsted, D.; McDermott, M. J.; Gallant, M.; Cubuk, E. D.; Merchant, A.; et al. An autonomous laboratory for the accelerated synthesis of novel materials. *Nature* **2023**, *624* (7990), 86−91.
(57) Delgado-Licona, F.; Alsaiari, A.; Dickerson, H.; Klem, P.; Ghorai, A.; Canty, R. B.; Bennett, J. A.; Jha, P.; Mukhin, N.; Li, J.; et al. Flow-driven data intensification to accelerate autonomous inorganic materials discovery. *Nature Chemical Engineering* **2025**, *2*, 436−446.

https://doi.org/10.1021/jacs.5c16416
J. Am. Chem. Soc. XXXX, XXX, XXX−XXX